This is the accepted manuscript made available via CHORUS. The article has been published as:

Finite-temperature elasticity of fcc Al: Atomistic simulations and ultrasonic measurements

Hieu H. Pham, Michael E. Williams, Patrick Mahaffey, Miladin Radovic, Raymundo Arroyave, and Tahir Cagin

Phys. Rev. B **84**, 064101 — Published 8 August 2011

DOI: 10.1103/PhysRevB.84.064101

Finite Temperature Elasticity of fcc Al: Atomistic Simulations and Ultrasonic Measurements

Hieu H. Pham[a], Michael E. Williams[b]. Patrick Mahaffey[c], Miladin Radovic[b,d],
Raymundo Arroyave[b,d], and Tahir Cagin[a,b,d]
[a] Dept. of Chemical Engineering, Texas A&M University, College Station, TX 77843, USA
[b] Dept. of Mechanical Engineering, Texas A&M University, College Station, TX 77843, USA
[c] Dept. of Industrial and Systems Engineering, Texas A&M University, College Station, TX 77843, USA
[d] Materials Science and Engineering Program, Texas A&M University, College Station, TX 77843, USA

Though not very often, in literature there are cases where discrepancies exist in temperature dependence of elastic constants of materials. A particular example of this case is the behavior of C_{12} coefficient of a simple metal, aluminum. Here, we attempt to provide insight into various contributions to temperature-dependence in elastic properties by investigating the thermo-elastic properties of fcc aluminum as a function of temperature through the use of two computational techniques and experiments. First, *ab initio* calculations based on density functional theory (DFT) are used in combination with quasi-harmonic theory to calculate the elastic constants at finite temperatures through a strain-free energy approach. Molecular dynamics (MD) calculations using tight-binding potentials are then used to extract the elastic constants through a fluctuation-based formalism. Through this dynamic approach, the different contributions (Born, kinetic and stress fluctuations) to the elastic constants are isolated and the underlying physical basis for the observed thermally-induced softening is elucidated. The two approaches are then used to shed light on the relatively large discrepancies in the reported temperature dependence of the elastic constants of fcc aluminum. Finally, the polycrystalline elastic constants (and their temperature dependence) of fcc aluminum are determined using Resonant Ultrasound Spectroscopy (RUS) and compared to previously published data as well as the atomistic calculations performed in this work.

I. INTRODUCTION

Development and selection of new materials requires accurate knowledge of their properties as well as reliable experimental and theoretical tools for their characterization. In the particular case of high-temperature structural materials, the component designer needs (at the very least) reliable information on their thermo-elastic behavior over a wide temperature range[1]. Although one may think that this information is readily available, the truth of the matter is that there are significant discrepancies among different experimental studies, even for the most widely used materials. The problem is even more daunting in the case of novel materials currently being under development for next-generation high-temperature structural materials, for example.

As an example, we summarize in Figure 1 published experimental data on the adiabatic C_{12} elastic constant of fcc aluminum as a function of temperature from four different studies[2-5]. In these studies, the elastic constants were determined by identifying the resonant frequencies of single crystalline specimens within the kHz-to-MHz range. In this figure, quantitative and even qualitative differences can be seen among the three different experimental data sets. While the measurements by Sutton[4], Kamm and Alers[3], and Gerlich[2] show a softening of this shear constant with increasing temperature, Tallon[5] (the most recent---and one would expect the most accurate---experimental work on elastic properties of aluminum) reports an actual increase of the C_{12} elastic constant with temperature. Although some of the discrepancies can be explained by the use of different frequency ranges (lower frequencies are used in the earlier study by Sutton[4]), the qualitative differences---softening vs. hardening---observed indicate significant systematic problems in at least one of the experimental investigations.

Given the fact that aluminum has been one of the most widely characterized and simulated metals[2, 4-12], these results are rather surprising. However, it is important to note that the accurate determination of elastic constants through resonance techniques is far from trivial[13], and the actual results are subject to non-negligible degrees of interpretation. Based on the published experimental results[2-5] alone, it is impossible to determine *a priori* which of the published data most accurately represents the actual thermo-elastic behavior of fcc aluminum. Moreover, the puzzling hardening of C_{12} reported by Tallon[5], if true, may indicate unexpected significant anharmonic phenomena in a metal that is normally considered to be slightly anharmonic at most. In this work, we try to address these important issues by using two different computational techniques---electronic structure calculations based on Density Functional Theory[14-16] as well as classical Molecular Dynamics (MD)---to determine the temperature dependence of the elastic tensor of aluminum and complement these simulations with state-of-the-art Resonant Ultrasound Spectroscopy (RUS) measurements[13, 17]. In the following sections, we will describe the different methods used as well as the results obtained. It is expected that the computational methodology presented in this work can in turn be used to assess the quality of published thermo-elastic data for other important high temperature structural materials and to reliably predict these properties in cases where no experimental information is available.

II. THERMODYNAMIC DEFINITIONS OF ELASTIC CONSTANTS

The adiabatic (C^{S}_{ijkl}) and isothermal (C^{T}_{ijkl}) second-order elastic constants can be defined as second derivatives of internal energy E and the Helmholtz free energy F, respectively, with respect to the homogeneous deformation of the unit cell[18].

$$C^{S}_{ijkl} = \frac{1}{V_0}\frac{\partial^2 E}{\partial \varepsilon_{ij}\partial \varepsilon_{kl}}, \text{ and } C^{T}_{ijkl} = \frac{1}{V_0}\frac{\partial^2 F}{\partial \varepsilon_{ij}\partial \varepsilon_{kl}} \tag{1}$$

where V_0 and ε_{ij} are the reference volume and strain tensor of the system, respectively.

In turn, the total free energy of a system is described by a Hamiltonian $\boldsymbol{H}$, which is the sum of kinetic energy and potential energy, for a two body form of interactions between particles can be written as:

$$H = \sum_{a=1}^{N} \frac{p_a^2}{m_a} + \sum_{a<b} U(r_{ab}) \tag{2}$$

where p_a and m_a correspond to momentum and mass of particle a, while r_{ab} corresponds to the interatomic separation between atom pairs a-b and U is the potential energy function.

Using the definition given above, the statistical fluctuation formula for second-order elastic constants can be derived and presented as follows[19, 20].

$$C_{ijkl} = \frac{2Nk_BT}{V_0}(\delta_{ik}\delta_{lj} + \delta_{il}\delta_{kj}) + \langle \chi_{ijkl} \rangle - \frac{V_0}{k_BT}\left(\langle \sigma_{ij}\sigma_{kl} \rangle - \langle \sigma_{ij} \rangle \langle \sigma_{kl} \rangle \right) \tag{3}$$

where N – number of particles, δ - Kronecker delta and σ - microscopic stress tensor.

The first term has a direct connection with temperature and corresponds to the kinetic energy contribution to the elastic tensor. The second one is called the Born term and is related to the strain derivative of the interaction potentials U:

$$\langle \chi_{ijkl} \rangle = \frac{1}{V_0} \frac{\partial^2 U}{\partial \varepsilon_{ij} \partial \varepsilon_{kl}} \tag{4}$$

in which the $\langle \ \rangle$ sign denotes ensemble averaging at the reference volume of the system. The averaging over an microcanonical (*NVE*) or canonical (*NVT*) ensemble will correspond to adiabatic or isothermal elastic constants, respectively.

The kinetic and Born terms contribute to the intrinsic stiffness of the crystal. The last term in Equation 3 corresponds to contributions from fluctuations in the microscopic stress tensor of the crystal. While the Born term can certainly be affected by anharmonic contributions to the free energy, it is the third term in which these contributions become more apparent. As will be shown in this work, stress fluctuation contributions can contribute significantly to the temperature dependence of the elastic tensor even in relatively simple systems such as aluminum.

III. DETERMINATION OF THERMO-ELASTIC PROPERTIES THROUGH DFT-BASED STATIC CALCULATIONS

A. Approach

At the most fundamental level, the elastic constants are related to the variation of interatomic forces with respect to atomic displacements. Over the past decades, many different approaches have been developed to predict the elastic properties of crystals through the use of atomistic calculations. Dynamic methods make full use of the fluctuation-based definition for the stiffness of the crystal described in Equation 3. Static methods, on the other hand, can only consider contributions to the stiffness tensor due to variations in the internal stress state of the crystal with respect to uniform crystal deformations without considering anharmonic atomic displacements away from equilibrium or (explicitly) fluctuations in the stress tensor. In these static techniques, only the so-called Born contribution to the elastic constants can be calculated directly. The individual components of the elastic constant tensor can be determined either by establishing relationships between strain and resulting internal stresses[21] or between the energy of the crystal and imposed strains[22]. Both static approaches can be trivially implemented within the context of DFT calculations.

In our DFT calculations, the elastic energy per crystal unit volume is expanded in terms of the strain state. Specifically, we calculate the variation in the energy of a crystal as a function of strain, under *constant volume constraints.*

$$E\left(e_i\right)=E_0+\frac{1}{2}V\sum C_{ij}e_ie_j+O\left[e_i^3\right] \tag{5}$$

By judiciously selecting the proper volume-conserving strain tensor, it is possible to establish a relationship between the difference in lattice energies with respect to unstrained state and the corresponding strain[23]. For example, in the case of crystals of cubic symmetry[23], the volume-conserving orthorhombic strain tensor:

$$
\begin{aligned}
&\varepsilon_1 = -\varepsilon_2 = x \\
&\varepsilon_3 = x^2 \big/ \left(1 - x^2\right) \\
&\varepsilon_4 = \varepsilon_5 = \varepsilon_6 = 0
\end{aligned}
\tag{6}
$$

can be used to establish a relationship between the change in lattice energy and the shear elastic constant $C_{11} - C_{12}$:

$$\Delta E(x) = V\left(C_{11} - C_{12}\right)x^2 + O\left[x^4\right] \tag{7}$$

Likewise, the C_{44} elastic constant can be obtained from volume-conserving monoclinic strains:

$$
\begin{aligned}
&\varepsilon_6 = x,\ \varepsilon_3 = x^2 \big/ \left(4 - x^2\right) \\
&\varepsilon_1 = \varepsilon_2 = \varepsilon_4 = \varepsilon_5 = 0
\end{aligned}
\tag{8}
$$

The corresponding lattice energy-strain relationship can in turn be used to determine C_{44}:

$$\Delta E(x) = \Delta E(-x) = VC_{44}\, x^2/2 + O\left[x^4\right] \tag{9}$$

The expression above is only applicable at 0 K, where contributions due to thermal excitations of vibrational, electronic, configurational and/or magnetic degrees of freedom are neglected. At finite temperatures, however, one has to take these contributions into account since straining the lattice would have an effect over thermally-excited degrees of freedom, particularly those related to lattice vibrations. In recent work, Ackland et al[24] have used a similar approach to investigate the elastic properties of high temperature metals and intermetallics.

In this work, we proceeded to impose volume-conserving strains necessary to extract the $C_{11} - C_{12}$ and C_{44} elastic constants. For each of the strained structures, the phonon density of states (DOS) was determined through the direct force-constant approach[25]. The resulting vibrational free energy was in turn calculated by using simple statistical mechanical formulas[6]. Although electronic contributions are not expected to be significant in aluminum due to relatively low electronic density at the Fermi level, the electronic free energy was calculated using the temperature-independent self-consistent one-electron approximation[26]. In order to take into account the effects of lattice thermal expansion, the quasi-harmonic approximation was used. In this approximation, it is assumed that the phonons (and electronic DOS) are only volume dependent[27].

For each of the volumes considered, the total free energy as a function of strain was used to calculate the corresponding elastic constants (replacing ΔE by ΔF_{Total} in the expressions above) at different temperatures. Within the quasi-harmonic approximation, a $C_{ij}(V,T)$ surface---for C_{11}-C_{12} and C_{44}, respectively---was then constructed. The resulting elastic tensor surface in *V-T* space was then represented mathematically using a two-dimensional spline (more details below). Using the volume expansion calculated from the *ab initio* total free energy calculations[6], the elastic constants at the *equilibrium volume at each temperature* were then calculated by evaluating the two-dimensional spline along the *V-T* path corresponding to the *predicted* volume thermal expansion derived from the quasi-harmonic approximation. In order to isolate C_{11} from C_{12}, the relationship between these elastic constants and the bulk modulus for cubic crystals was used ($B=(C_{11}+2C_{12})/3$). The bulk modulus was in turn calculated by fitting an equation of state of the form[28]:

$$E(V)=a+bV^{-1/3}+cV^{-2/3}+dV^{-1} \tag{10}$$

where *a, b, c, d* are fitting parameters. These parameters can then be related to cohesive energy, E_0; equilibrium volume, V_0; bulk modulus, B_0 and pressure derivative of the bulk modulus, B'. For the detailed mathematical relations between the fitting coefficients of the equation of state used and the corresponding state variables the reader is referred to the work by Shang and Böttger[28]. The particular choice of the equation of state did not greatly affect the results obtained in this work and comparisons with more conventional expressions (such as Birch and Birch-Murnaghan) resulted in no major differences. The particular reason for the selected EOS form was based on mathematical convenience when fitting quasi-harmonic free energies over the temperature range of interest.

The elastic constants calculated from this approach correspond to isothermal conditions. In contrast, resonance-based experiments are performed under adiabatic conditions and thus the following thermodynamic conversion must be used[29]:

$$C_{ij}^{S} = C_{ij}^{T} + \frac{V\lambda_i\lambda_j T}{C_v} \tag{11}$$

In cubic crystals, for C_{11} and C_{12}, $\lambda_i = \lambda_j = \alpha\left(C_{11}^{T} + 2C_{12}^{T}\right)$[30]. In the case of C_{44}, the coefficients λ_4 are zero due to the symmetry of the thermal expansion coefficient tensor and thus there is no difference between the isothermal and adiabatic constants. This fact is highly useful when trying to compare the results from calculations with experimental measurements in a direct manner.

B. Results

The calculations were performed using projector-augmented plane wave pseudopotentials (PAW) as implemented in the electronic structure code VASP[31, 32]. All the calculations were performed within the GGA approximation with the parameterization suggested by Perdew and Wang (PW91)[33]. For these calculations, the electrons in the configuration $3s^2 3p^1$ were considered valence states. In all calculations, the k-point mesh consisted of at least 10,000 k-points per reciprocal atom. The particular shape of the k-point mesh was adjusted depending on the symmetry of the reciprocal lattice of the structures considered. The energy cutoff used was 350 eV. The k-point density and energy cutoff employed ensured a very good convergence (within less than 0.1meV) of the total energies.As mentioned above, the quasi-harmonic approximation was used to calculate the thermodynamic properties---including volume thermal expansion and bulk modulus---of fcc aluminum. Seven volumes (ranging from -1 % to 5 % lattice expansion) were considered in our calculations. For each volume, we used the so-called ‘direct method’ to obtain the phonon density of states. The lattice dynamics calculations used to determine the phonon density of states were performed using the ATAT code [34, 35], using supercells containing 32 atoms. From these calculations, the free energy (including contributions due to electronic degrees of freedom) can be easily calculated using the standard statistical mechanics formulas[6]. The reader is referred to the article by one of the co-authors[6] for a more detailed comparison between calculated and experimental thermodynamic properties of fcc Al.

As mentioned above, we used volume-conserving strains to obtain the C_{11}-C_{12} and C_{44} elastic constants. To calculate C_{11}-C_{12} *at each volume,* we used seven volume-conserving tetragonal strains (see Equations 6 and 7) with the strain parameter, x, ranging from -0.06 to 0.06. For C_{44}, *at each volume*, we used five volume-conserving monoclinic strains (see Equations 8 and 9) with the strain parameter, x, ranging from 0 to 0.06. In both sets of calculations, the strain parameter was equally spaced. For each strain state, we calculated its vibrational and electronic free energies as described above. By combining the elastic constants calculated at different temperatures and volumes, we created a V-T surface for C_{11}-C_{12} and C_{44}. The V-T surface was represented mathematically through the use of a 2-D smooth B-spline (using the *interpolate* module in scipy[36]). The temperature dependence of the elastic constants was then obtained by evaluating the 2-D spline along the V-T path resulting from the predicted thermal expansion for fcc aluminum. Finally, we applied the conversion (see Equation 11) from isothermal to adiabatic elastic constants in order to compare our calculations with experiments. We would like to note that the use of the smooth 2-D spline also contributed to the reduction in the noise associated with the calculation of the elastic tensor and this is the main reason for the low level of noise in the temperature dependence of the elastic tensor calculated through DFT+quasi-harmonic approximations.

Table I shows comparisons between calculated and experimental structural and thermodynamic properties of fcc Al. In general, the calculated structural and thermodynamic properties agree very well with experiments. In the table, we also present the calculated elastic constants (at 0 K) using two different approaches: one based on energy-strain fits[23]---used in the rest of the present article---and the other one based on stress-strain relations[21]. The table show that both sets of calculations (using the same k-point mesh density, energy cutoff and convergence criteria described above) yielded results relatively close to experiments (within ~5 GPa) as well as to one another (within ~

2 GPa). Since these two calculation schemes are fundamentally independent of one another, the agreement suggests the calculations are already well converged with respect to k-point mesh and energy cutoff. Other calculations performed at different strain levels (for the stress-strain calculations) and maximum strains (for the energy-strain fits) suggest convergence within ± 1 GPa.

After applying the corrections outlined above, we proceeded to compare the resulting temperature dependence of the elastic constants with the published data. Figure 2 compares C_{11} as obtained from experiments[2-5] with the DFT calculations. In the figure, we include the calculated C_{11} obtained simply by finding the value of this elastic constant at different volumes through the 0 K energy-strain relations (cold curve), as well as the C_{11} in which we used the free energy-strain relations (quasi-harmonic). From the figure it is seen that only by considering the vibrational contributions to the total free energy of the strained structures it is possible to closely reproduce the temperature dependence of C_{11} as reported by Gerlich[2] and Kamm and Alers[3] as well as (in a limited manner) the results by Tallon[5].

In Figure 3, the (cold curve) C_{12} shows a softening close to that reported by Gerlich[2] and Kamm and Alers[3]. Surprisingly, our calculations suggest that vibrational contributions lead to a stiffening of C_{12}. In this case, the quasi-harmonic C_{12} remains almost constant as temperature increases, in contrast with what Gerlich[2] and Kamm and Alers[3] suggest. Our results seem to suggest that Sutton[4] overestimated the temperature dependence of this elastic constant. The hardening of C_{12} with temperature reported by Tallon[5] is not supported by our calculations, even considering the relatively small softening resulting from our quasi-harmonic calculations. It is likely that the underestimation of softening in our quasi-harmonic calculations results from the small supercells used to calculate the strain free energies. As will be seen in the next section, fluctuations in the microscopic stress tensor have very limited effects on the softening of this component of the stiffness tensor. Thus, this softening originates from the weakening of the interatomic force constants as volume increases, and is thus mostly due to Born-like contributions.

In Figure 4, we present the comparison between calculated and experimental adiabatic elastic constants including only the results published by Gerlich[2] and Kamm and Alers[3]. The figure shows that the temperature dependence of (quasi-harmonic) C_{11} agrees rather well with the experiments (in this figure we exclude the results reported by Sutton[4] and Tallon[5]). The figure shows that the quasi-harmonic calculations differ from experiments by an almost constant amount. This discrepancy is likely due to the underestimation of the bulk modulus calculated within the GGA approximation, as discussed earlier.

Figure 4 shows that the agreement is also quite good for C_{44}. This elastic constant is not affected by the underestimation of the bulk modulus and in this case, the (cold curve) and quasi-harmonic calculations show virtually no difference. Despite these promising results, our calculations still underestimate the softening in C_{12} reported by Gerlich[2] and Kamm and Alers[3].

Given the good agreement between the DFT calculations and at least two experimental data sets, one would be tempted to conclude that full consideration of dynamic, anharmonic contributions to the stiffness tensor are not important. In fact, even though fcc aluminum appears to be a weakly anharmonic crystal, Forsblom et al[9] have in fact shown that aluminum is highly anharmonic at even moderate temperatures. What contributes to the apparent non-anharmonicity of this crystal is the almost complete cancellation of anharmonic contributions of opposite signs. If anharmonic contributions in fact are important in fcc aluminum, the good agreement between the DFT calculations and the experiments by Gerlich[2] could be due to fortuitous error cancellations. To further investigate this possibility, in the next section we employ dynamic methods to estimate the elastic stiffness tensor through the fluctuation formulas presented in Equation 3.

IV. DETERMINATION OF THERMO-ELASTIC PROPERTIES THROUGH MOLECULAR DYNAMICS CALCULATIONS

A. Approach

We performed molecular dynamics (MD) calculations on the elastic constants of Al using tight-binding potentials suggested by Rosato et al, which is often referred as RGL[37, 38]. Although simpler pair potentials for fcc Al have been successfully developed, they still fail to fully reproduce the physical properties of crystalline materials, as the role of electron density and the atomic bonding in pair potentials are underestimated. For instance, pure pair potentials imply the Cauchy relation between elastic constants $C_{12} = C_{44}$, which is not necessarily true in real metals and alloys. Also, stacking fault energies, surface structure and relaxation properties cannot be accurately estimated while using pair potentials[37]. Many-body models overcome these limitations by properly treating the essential band character of the metallic bonding. Over the past decades, a collection of many-body potentials has been developed, including those based on effective medium theory[39], embedded atom method[40], as well as those based on the tight-biding approach, such as the Finnis and Sinclair[41], Sutton and Chen[42] and the RGL model [37, 38].

The tight-binding methods describe interatomic interactions as a combined effect of a short-range pair-wise repulsion and a many-body density dependent cohesion. The functional form of RGL interaction potential for an atom ***a*** can be described as follows[37, 38]:

$$E_a = AV(r_{ab}) - \xi\rho_a \tag{12}$$

in which

$$\begin{aligned} V(r_{ab}) &= \sum_{b\neq a} \exp(-p(\frac{r_{ab}}{r_0}-1)), \\ \rho_a &= (\sum_{b\neq a} \phi(r_{ab}))^{1/2}, \\ \phi(r_{ab}) &= \exp(-2q(\frac{r_{ab}}{r_0}-1)) \end{aligned}$$

where r_0 is the first neighbor atomic distance, and A, ζ, p, q are empirical parameters whose values are obtained by fitting to 0 K properties such as cohesive energy, elastic coefficients and structure stability and they are all published in the work of Cleri et al[37].

Compared to the Sutton-Chen scheme, which has been successfully utilized to study various bulk properties of metal and metal alloys[43-48], the RGL model is fairly similar in terms of its functional expression and number of fitting parameters. The first term in Equation 12 indicates the atomic repulsions that take into account the increase in kinetic energy of bonding electrons when two ions get close to each other. The Sutton-Chen model introduces a power form instead of an exponential expression to describe these ion-ion repulsions. The second term, having a general formulation of the type $-\zeta\left[\sum_{b\neq a}\varphi(r_{ab})\right]^{1/2}$, specifies a many-body cohesion that accounts for the nature of the effective band energy and it balances with repulsion forces in order to stabilize the crystals. The function $\varphi(r_{ab})$ corresponds to the local electronic charge density induced at site ***a*** from atoms at site ***b***, and is also described by a power function in the case of the Sutton-Chen model.

Our MD simulation model consists of 500 Al atoms, in which the cut-off distance covers up to the fifth nearest neighbor[49] (corresponding to $a\sqrt{5/2}$ in fcc crystals), and the simulation time step is chosen to be 1 fs. At first, a thermalization process is conducted by slowly heating the system from 0.001 K (with the temperature increment of 1 K per step) until it reaches the desired temperature. The zero strain state is determined from constant temperature and stress ensembles, by changing the volume of the supercell. Once the reference volume has been obtained, a strict velocity scaling of 50,000 steps is performed, followed by a preliminary molecular dynamics run of 20,000 steps to equilibrate the system at the temperature of interest. The elastic constants are then derived from the second derivative of the total energy with respect to the homogeneous deformation of unit cell, as given in Equation 3, by performing 250,000 steps of constant shape and constant energy simulations (*EhN* ensemble). The nine elastic constants were calculated separately in order to ensure convergence. It was then verified that the resulting stiffness tensor's symmetry was cubic (i. e. non-vanishing C_{11}, C_{12}, and C_{44}).

B. Results

The MD simulations show that the elastic constants of Al decrease with temperature, as a softening in materials is expected. This is in agreement with the DFT calculations as well as with the experimental results by Gerlich[2] and Sutton[4]. The stability criteria for cubic crystals was held for Al, as $C_{44}>0$, $C_{11}>0$ and $C_{11}>C_{12}$. As demonstrated in Figure 8, C_{44} declines and the divergence between C_{11} and C_{12} diminishes as temperature increases. Beyond the equilibrium melting point, vanishing C_{11}-C_{12} and C_{44} would correspond to Born melting.

The kinetic energy, Born term and fluctuation contributions are listed (Table II) and plotted separately (Figures 5-7) in order to elucidate their individual contributions to the stiffness tensor. As can be seen in Figure 5, the kinetic contributions are rather small, compared to the other two terms, and even vanish for C_{12} . Although the kinetic term contributes to a stiffening of C_{11} and C_{44}, its relative contribution to the total elastic constants (Table II and Figure 8) is insignificant.

By examining Table II, it can be seen that the Born term (Figure 6) constitutes the most important contribution to the stiffness tensor. Table III also suggests that this term has almost the same temperature dependence for all three elastic constants. Our calculations indicate that the Born term of stiffness tensor softens as temperature increases, which is consistent with weakening of interatomic bonds as interatomic distance increases. The fluctuation term (Figure 7) represents the contributions to the stiffness tensor due to fluctuations in the microscopic stress tensor. Since these fluctuations are related to the amplitude of atomic displacements, as temperature increases fluctuation contributions to the stiffness tensor also increases. Table III shows that fluctuation contributions to the temperature dependence are strongest for C_{11}, almost comparable to the temperature dependence of the Born contribution. In the case of C_{12} and C_{44}, the temperature dependence of the fluctuation term is 100 and 10 times weaker than the corresponding Born term, respectively.

Since the temperature dependence of the Born term is similar for all the elastic coefficients and the contributions from kinetic energy terms are relatively small, the difference in the temperature dependence of the total elastic constants is mostly determined by the behavior of the fluctuation components. Those contributions increase continuously and get up to about 18 % and 29 % of the Born terms for C_{11} and C_{44}, respectively, at 900 K (which is slightly below the experimental melting point of aluminum). In contrast, fluctuation terms in the C_{12} constant are almost negligible. Figure 8 shows clearly a linear dependence of elasticity with respect to temperature in the region after room temperature up to 900 K. Also, the slopes of C_{11}, C_{12} and C_{44} with respect to temperature reported by these molecular dynamics calculations are in relatively good agreement (see Tables III) with those obtained from our earlier DFT calculations. In fact, the major disagreement between the classical MD and DFT calculations corresponds to the low temperature C_{12} elastic constant, with C_{44} differing by less than 10 % and C_{44} agreeing almost perfectly.

V. DETERMINATION OF ELASTIC MODULI BY RESONANT ULTRASOUND SPECTROSCOPY

A. Approach

RUS is a high-precision dynamic technique that allows determination of up to 9 elastic constants by measuring vibrational spectrum of the samples with known geometry --- usually in the shape of parallelepipeds or cylinder --- and mass[13, 50].

A polycrystalline aluminum sample (Metalman, Long Island City, NY) with purity of 99.999 % and density of 2.689 g/cm^3 was used in the present study to determine elastic moduli and compare to the results of DFT and MD calculations. The sample was precisely machined in the form of discs with average diameter of 28.052 mm and average thickness of 3.270 mm. The Young's (E) and shear (μ) moduli of the sample were determined using Resonant Ultrasound Spectroscope (RUS) (Magnaflux Quasar, Albuquerque, NM). The details of the experimental set up for RUS can be found elsewhere[13, 51, 52]. Briefly, the disc shaped sample was supported by three piezoelectric transducers. One transducer (transmitting transducer) generates an elastic wave of constant amplitude but of varying frequency (covering a large number of vibrational eigenmodes of the sample). The resonance response of excited sample is detected by the other two transducers, i.e. receiving transducers. In order to study the variation of elastic moduli as a function of temperature, the commercially available setup for RUS at room temperature was modified for high temperature measurements in which 4 inches long SiC extension rods were used to transmit the ultrasound waves to and from sample at desired temperature in the furnace, while keeping the piezoelectric transducers out of the furnace, thus unaffected by high temperature. The sample was heated at a ramping rate of 10 K/min in argon atmosphere and resonance spectra were collected at an interval of 50 K, from room temperature up to 773 K after an isothermal hold of 10 minutes.

The resonant spectra were collected in the 10-200 kHz frequency range to cover the first 40 eigenfrequencies. With known dimensions, density, and a set of "guessed" elastic constants --- i.e. C_{11} and C_{44} considering the material as an isotropic solid --- accurate elastic moduli of the solid can be determined from collected RUS spectra using a multidimensional, iterative fitting approach (RuSpec (Magnaflux Quasar, Albuquerque, NM) that minimizes the root-mean-square (RMS) error between the measured and calculated resonant frequencies for a sample of known mass and dimensions. The calculated resonant frequencies were determined by minimization of the Lagrangian equation corresponding to the free body vibrations of an elastic solid, using Rayleigh-Ritz method[50, 53].

B. Results

Figure 9 shows the measured Young's and shear moduli and Poisson's ratio of the polycrystalline aluminum sample as determined by RUS over the 297-773 K temperature range. In order to compare these new measurements with the elastic constant tensor calculated in this work and measured previously[2-5], the single crystal elastic tensor was transformed to polycrystalline elastic constants through Voigt-Reuss-Hill[54]averaging.

Figures 9 and 10 clearly shows a very good agreement between the DFT calculations and the experimental measurements by Gerlich and the RUS results obtained in this work. The RUS measurements for polycrystalline aluminum in this work differ by less than about 2 GPa at the highest temperatures measured. The (cold curve) DFT calculations slightly overestimate the Young's and shear modulus (compared to the experimental results) and underestimate Poisson's ratio, although the calculated temperature dependence agrees very well with the experimental data sets used for comparison. The (quasi-harmonic) DFT calculations yield Young's and shear modulus within the ranges measured by Gerlich as well as with the measurements reported in this work. However, an inflection at about 600 K takes these polycrystalline elastic constants closer to those predicted by our MD calculations.

Figure 9 shows that the Molecular Dynamics simulations exhibit the largest discrepancy with the polycrystalline elastic moduli and Poisson's ratio derived from the measurements by Gerlich and this work. As described above, the major reason for this discrepancy is an overestimation (of about 20 %) of the low temperature C_{12} coefficient. Despite this discrepancy, Figure 9 shows that the temperature dependence of the averaged polycrystalline elastic constants derived from the MD calculations agree very well with the experiments (as well as with the DFT calculations).

VI. CONCLUSIONS

This paper was motivated by the significant quantitative and qualitative discrepancies in the finite temperature elastic constants of fcc Al measured by three different groups. Given the fact that aluminum is one of the most technologically important and well characterized metals, the discrepancies were very surprising. While a priori it is not possible to judge the reliability of a particular data set, we have demonstrated in this work how we can use atomistic simulation techniques to assess the reliability of experimental data.

Our DFT calculations exhibit surprisingly good agreement with the measurements by Gerlich[2] and by this study, even though these calculations neglected to consider anharmonic contributions to the stiffness tensor. Although this good agreement seems to suggest that fcc Al is at most weakly anharmonic, results by others[9] suggest that what seems to happen is that anharmonic contributions at least partially cancel out.

Our MD calculations consider all the possible contributions to the stiffness tensor. These calculations suggest that anharmonic contributions (manifested in the fluctuation term) seem to contribute significantly to the temperature dependence of the elastic constants, particularly C_{11}. These anharmonic effects are partly cancelled by the intrinsic kinetic stiffness of the crystal. While the calculated C_{12} obtained through MD simulations is significantly higher than the DFT-calculated and experimentally measured elastic constant, C_{11} and C_{44} agree well with the DFT calculations (errors of less than 10 %). In fact, MD and DFT calculations predict a change between 300 K and 900 K of around 17, 9 and 10 GPa for C_{11}, C_{12} and C_{44}, respectively. More importantly, this is also what we can extract from the data reported by Gerlich.

Finally, the calculated and averaged elastic constants in this work agree very well (at least with regards to the temperature dependence) with the experiments by Gerlich as well as the measurements performed in this work through RUS. Discounting the discrepancies in the MD-derived polycrystalline elastic moduli due to overestimation of the low temperature C_{12}, this work illustrates a sound methodology for the assessment of the quality of published thermo-elastic data for other important high temperature structural materials.

ACKNOWLEDGEMENTS

HHP and TC would like to acknowledge partial support for this research through ARO MURI (Anthenien) and ONR (N000140811054). Molecular Dynamics simulations have been carried out at the facilities of Laboratory of Computational Engineering of Nanomaterials. RA acknowledges the support from NSF through grants CMMI-0758298, 1027689, 0953984, 0900187, DMR-0805293 and CBET-0932249. First-principles calculations were carried out in the Chemical Engineering Cluster and the Super-Computer Facility of Texas A&M University as well as in the Ranger Cluster at the Texas Advanced Computing Center. Preparation of the input files and analysis of the data have been performed within the framework AFLOW/ACONVASP[55] developed by

Stefano Curtarolo as well as with the ATAT package[34, 35] developed by Axel van de Walle.

References

[1] M. Osawa, H. Shiraishi, T. Yokokawa, H. Harada, and T. Kobayashi, in *Superalloys 2004*, edited by K. A. Green, T. M. Pollock, H. Harada, T. E. Howson, R. C. Reed, J. J. Schirra and S. Walston (TMS (The Minerals, Metals & Minerals Society), 2004), p. 977.

[2] D. Gerlich and E. Fisher, J. Phys. Chem. Solids **30**, 1197 (1969).

[3] G. Kamm and G. Alers, J. Appl. Phys. **35**, 327 (1964).

[4] P. Sutton, Phys. Rev. **91**, 816 (1953).

[5] A. Tallon, J. Phys. Chem. Solids **40**, 831 (1979).

[6] R. Arroyave, D. Shin, and Z. Liu, Acta Mater. **53**, 1809 (2005).

[7] F. Cleri and V. Rosato, Phys. Rev. B **48**, 22 (1993).

[8] M. Forsblom and G. Grimvall, Phys. Rev. B **72**, 132204 (2005).

[9] M. Forsblom, N. Sandberg, and G. Grimvall, Phys. Rev. B **69**, 165106 (2004).

[10] B. Grabowski, L. Ismer, T. Hickel, and J. Neugebauer, Phys. Rev. B **79**, 134106 (2009).

[11] M. Kresch, M. Lucas, O. Delaire, J. Y. Y. Lin, and B. Fultz, Phys. Rev. B **77**, 024301 (2008).

[12] M. Zoli and V. Bortolani, J. Phys. Condens. Matter **2**, 525 (1990).

[13] M. Radovic, E. Lara-Curzio, and L. Riester, Mater. Sci. Eng. **A368**, 56 (2004).

[14] P. Hohenberg and W. Kohn, Phys. Rev. **136**, B864 (1964).

[15] W. Kohn, A. D. Becke, and R. G. Parr, J. Phys. Chem **100**, 974 (1996).

[16] W. Kohn and L. J. Sham, Phys. Rev. **140**, A1133 (1965).

[17] M. Radovic and E. Lara-Curzio, J. Am. Ceram. Soc. **87**, 2242 (2004).

[18] D. C. Wallace, *Thermodynamics of Crystals* (Wiley, New York, 1972).

[19] T. Cagin and J. R. Ray, Phys. Rev. B **38**, 7940 (1988).

[20] T. Cagin and J. R. Ray, Phys. Rev. B **37**, 699 (1988).

[21] Y. Le Page and P. Saxe, Phys. Rev. B **65**, 104104 (2002).

[22] Y. Le Page and P. Saxe, Phys. Rev. B **63**, 174103 (2001).

[23] M. Mehl, B. M. Klein, and D. A. Papaconstantopoulos, in *Intermetallic Compounds: Principles and Practice*, edited by J. H. Westbrook and L. Fleischer (John Wiley and Sons, London, 1993).

[24] G. J. Ackland, X. Huang, and K. M. Rabe, Phys. Rev. B **68**, 214104 (2003).

[25] A. van de Walle and G. Ceder, Rev. Mod. Phys. **74**, 11 (2002).

[26] M. Asta and V. Ozolins, Phys. Rev. B **64**, 094104 (2001).

[27] A. A. Quong and A. Y. Liu, Phys. Rev. B **56**, 7767 (1997).

[28] S. Shang and A. J. Bottger, Acta Mater. **53**, 255 (2005).

[29] P. Bruesch, *Phonons, Theory and Experiments* (Springer-Verlag, New York, 1982).

[30] W. P. Mason, *Piezoelectric Crystals and Their Applications to Ultrasonics* (D. Van Nordstan Co., New York, 1950).

[31] G. Kresse and J. Furthmüller, Comput. Mat. Sci. **6**, 15 (1996).

[32] G. Kresse and D. Joubert, Phys. Rev. B **59**, 1758 (1999).

[33] J. Perdew and Y. Wang, Phys. Rev. B **46**, 12947 (1992).

[34] A. van de Walle, M. Asta, and G. Ceder, CALPHAD: Comput. Coupling Phase Diagrams Thermochem. **26**, 539 (2002).

[35] A. van de Walle and G. Ceder, J. Phase Equilib. **23**, 348 (2002).

[36] E. Jones, T. Oliphant, and P. Peterson, URL http://www. scipy. org (2001).

[37] F. Cleri and V. Rosato, Phys. Rev. B **48**, 22 (1993).

[38] V. Rosato, M. Guillope, and B. Legrand, Philos. Mag. A **59**, 321 (1989).

[39] J. K. Norskov, Phys. Rev. B **26**, 2875 (1982).

[40] M. S. Daw and M. I. Baskes, Phys. Rev. B **29**, 6443 (1984).

[41] M. W. Finnis and J. E. Sinclair, Philos. Mag. A **50**, 45 (1984).

[42] A. P. Sutton and J. Chen, Philos. Mag. Lett. **61**, 139 (1990).

[43] T. Cagin, G. Dereli, M. Uludogan, and M. Tomak, Phys. Rev. B **59**, 3468 (1999).

[44] G. Dereli, T. Cagin, M. Uludogan, and M. Tomak, Philos. Mag. Lett. **75**, 209 (1997).

[45] H. H. Kart, M. Tomak, and T. Cagin, Model. Simulat. Mater. Sci. Eng. **13**, 657 (2005).

[46] H. H. Kart, M. Tomak, M. Uludogan, and T. Cagin, Int. J. Mod. Phys. B **18**, 2257 (2004).

[47] H. H. Kart, M. Tomak, M. Uludogan, and T. Cagin, Comput. Mater. Sci. **32**, 107 (2005).

[48] S. O. Kart, M. Tomak, M. Uludogan, and T. Cagin, Mater. Sci. Eng. A **435**, 736 (2006).

[49] F. Cleri and V. Rosato, Philos. Mag. Lett. **67**, 369 (1993).

[50] A. Migliori and J. L. Sarrao, *Resonant Ultrasound Spectroscopy: Applications to Physics, Materials Measurements, and Nondestructive Evaluation* (John Wiley and Sons, Inc. , 1997).

[51] M. Radovic, M. W. Barsoum, A. Ganguly, T. Zhen, P. Finkel, S. R. Kalidindi, and E. Lara-Curzio, Acta Mater. **54**, 2757 (2006).

[52] M. Radovic and E. Lara-Curzio, Acta Mater. **52**, 5747 (2004).

[53] W. M. Visscher, A. Migliori, T. M. Bell, and R. A. Reinert, J. Acoust. Soc. Am. **90**, 2154 (1991).

[54] R. Hill, Proc. Phys. Soc., London, Sect. A **65**, 349 (1952).

[55] W. Setyawan and S. Curtarolo, Comput. Mater. Sci. **49**, 299 (2010).

[56] Inorganic Crystal Structure Database (ICSD), http://www.fiz-karlsruhe.de/icsd_content.html (2010).

[57] G. Simmons and H. Wang, *Single Crystal Elastic Constants and Calculated Aggregate Properties: A Handbook* (The MIT Press, 1971).

[58] F. Nix and D. MacNair, Phys. Rev. **60**, 597 (1941).

[59] M. Chase Jr and C. Davies, J. Phys. Chem. Ref. Data **14**, 1856 (1985).

[60] Periodic Table, http://www.infoplease.com/periodictable.php?id=13 (2010).

List of Tables and Figures

TABLE I. Comparison between experimental and calculated properties of fcc aluminum.

TABLE II. Molecular Dynamics and Quasi-harmonic DFT calculations of aluminum second-order elastic constants.

TABLE III. Average temperature dependence of elastic constants. Comparison between MD and DFT calculations.

FIG. 1. (color online) Experimental[2-5] adiabatic C_{12} elastic constant as a function of temperature.

FIG 2. (color online) Experimental[2-5] and DFT calculated C_{11} adiabatic elastic constant. For the curve labeled as 'cold curve' (solid, blue line), the elastic constants where calculated from the strain-energy relations at 0 K at different volumes. Ab initio-calculated volume expansion was then used to convert volume to temperature dependence. The curve labeled as quasi-harmonic was obtained from strain-free energy relations.

FIG. 3. (color online) Experimental[2-5] and DFT calculated C_{12} adiabatic elastic constant. For the curve labeled as 'cold curve' (solid, blue line), the elastic constants where calculated from the strain-energy relations at 0 K at different volumes. Ab initio-calculated volume expansion was then used to convert volume to temperature dependence. The curve labeled as quasi-harmonic was obtained from strain-free energy relations.

FIG. 4. (color online) DFT calculated and experimental[2, 3] adiabatic elastic constants of fcc Al. For the curves labeled as 'cold curve' (solid, blue line), the elastic constants where calculated from the strain-energy relations at 0 K at different volumes. Ab initio-calculated volume expansion was then used to convert volume to temperature dependence. The curves labeled as quasi-harmonic was obtained from strain-free energy relations.

FIG. 5. (color online) Kinetic energy contributions to C_{11}, C_{12}, C_{44} as a function of temperature in MD calculations.

FIG. 6. (color online) Born term contributions to C_{11}, C_{12}, C_{44} as a function of temperature in MD calculations.

FIG. 7. (color online) Fluctuation term contributions to C_{11}, C_{12}, C_{44} as a function of temperature in MD calculations.

FIG. 8. (color online) MD calculations on C_{11}, C_{12}, C_{44} at elevated temperatures.

FIG. 9. (color online) Polycrystalline Young's (a) and shear modulus (b). The averaged elastic constants from experimental results by Gerlich[2] as well as those measured in this work through RUS are compared to DFT and classical MD calculations.

FIG. 10. (color online) Polycrystalline Poisson's ratio. The averaged elastic constants from experimental results by Gerlich[2] as well as those measured in this work through RUS are compared to DFT and classical MD calculations.

TABLE I. Comparison between experimental and calculated properties of fcc aluminum.

Property	Experiment	Calculations	Units
a	4.046[56]	4.050	Å
$B_{0\,\mathrm{K}}$	79[57]	72	GPa
$B_{298\,\mathrm{K}}$	76[2]	67	GPa
$C_{11,\,0\,\mathrm{K}}$	107[57]	105[a],103[b]	GPa
$C_{12,\,0\,\mathrm{K}}$	61[57]	54[a],56[b]	GPa
$C_{44,\,0\,\mathrm{K}}$	28[57]	26[a],30[b]	GPa
$\alpha_{298\,\mathrm{K}}$	23 [58]	25	$\mathrm{x}10^{-6}/\mathrm{K}$
$C_{p},_{298\,\mathrm{K}}$	24.3[59]	24.4	J/(mol K)
$S_{298\,\mathrm{K}}$	28.4[59]	29.5	J/(mol K)
Debye temperature, Θ	394[60]	381	K

[a] Elastic constants were calculated using stress-strain relations[21]

[b] Elastic constants were calculated using energy-strain fits[23]

TABLE II. Molecular Dynamics and Quasi-harmonic DFT calculations of aluminum second-order elastic constants.

T, K	EC, GPa	MD				DFT	
		Kinetic energy	Born	Fluctuation	Total	Cold Curve	Quasi-harmonic
0	C_{11}	0.00	95.02	0.00	95.02	103.89	103.35
	C_{12}	0.00	74.40	0.00	74.40	55.88	56.16
	C_{44}	0.00	37.16	0.00	37.16	29.51	29.90
50	C_{11}	0.17	94.12	-0.71	93.58	103.59	102.71
	C_{12}	0.00	73.70	-0.05	73.65	56.05	56.32
	C_{44}	0.08	36.68	-0.42	36.34	29.20	29.60
100	C_{11}	0.32	93.73	-1.40	92.65	103.08	101.80
	C_{12}	0.00	73.30	-0.08	73.21	56.13	56.44
	C_{44}	0.16	36.43	-0.90	35.69	28.82	29.10
200	C_{11}	0.64	92.05	-2.64	90.06	101.54	99.21
	C_{12}	0.00	71.96	-0.23	71.73	56.07	56.57
	C_{44}	0.32	35.53	-1.72	34.13	27.86	27.64
300	C_{11}	0.98	90.45	-4.27	87.15	99.41	95.79
	C_{12}	0.00	70.56	-0.28	70.29	55.74	56.55
	C_{44}	0.49	34.58	-2.78	32.29	26.68	25.72
400	C_{11}	1.29	89.16	-5.90	84.55	96.82	91.76
	C_{12}	0.00	69.39	-0.41	68.99	55.21	56.41
	C_{44}	0.65	33.83	-3.54	30.93	25.33	23.56
500	C_{11}	1.62	87.53	-7.42	81.73	93.93	87.35
	C_{12}	0.00	67.94	-0.38	67.57	54.54	56.17
	C_{44}	0.81	32.87	-4.60	29.07	23.85	21.35
600	C_{11}	1.91	86.15	-9.05	79.02	90.85	82.79
	C_{12}	0.00	66.66	-0.44	66.22	53.80	55.84
	C_{44}	0.96	32.03	-5.39	27.59	22.28	19.30
700	C_{11}	2.21	84.48	-10.97	75.71	87.74	78.28
	C_{12}	0.00	65.13	-0.54	64.60	53.04	55.44
	C_{44}	1.10	31.01	-6.29	25.82	20.66	17.61
800	C_{11}	2.50	83.02	-12.99	72.53	84.72	74.07
	C_{12}	0.00	63.62	-0.73	62.89	52.32	54.99
	C_{44}	1.25	30.02	-7.27	23.99	19.04	16.50
900	C_{11}	2.81	81.77	-15.16	69.42	81.95	70.37
	C_{12}	0.00	62.08	-0.65	61.43	51.72	54.51
	C_{44}	1.41	29.03	-8.54	21.89	17.47	16.16

TABLE III. Average temperature dependence of elastic constants. Comparison between MD and DFT calculations.

	MD				DFT	
	kinetic	Born	fluctuation	total	Cold curve	Quasi-harmonic
ΔC_{11}, GPa	2.8	-13.3	-15.2	-25.6	-21.9	-33.0
dC_{11}/dT	3.1E-03	-1.5E-02	-1.7E-02	-2.8E-02	-2.4E-02	-3.7E-02
ΔC_{12}, GPa	0.0	-12.3	-0.7	-13.0	-4.2	-1.7
dC_{12}/dT	0.0E+00	-1.4E-02	-7.2E-04	-1.4E-02	-4.6E-03	-1.8E-03
ΔC_{44}, GPa	1.4	-8.1	-8.5	-15.3	-12.0	-13.7
dC_{44}/dT	1.6E-03	-9.0E-03	-9.5E-03	-1.7E-02	-1.3E-02	-1.5E-02

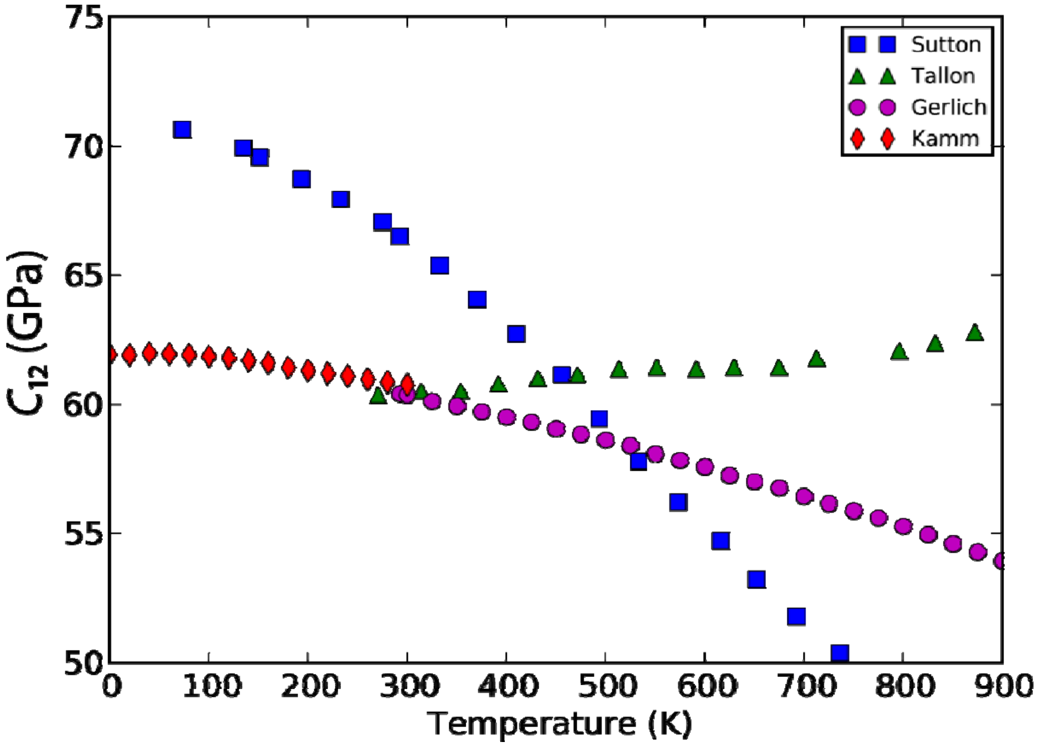

FIG. 1. (color online) Experimental[2-5] adiabatic C_{12} elastic constant as a function of temperature.

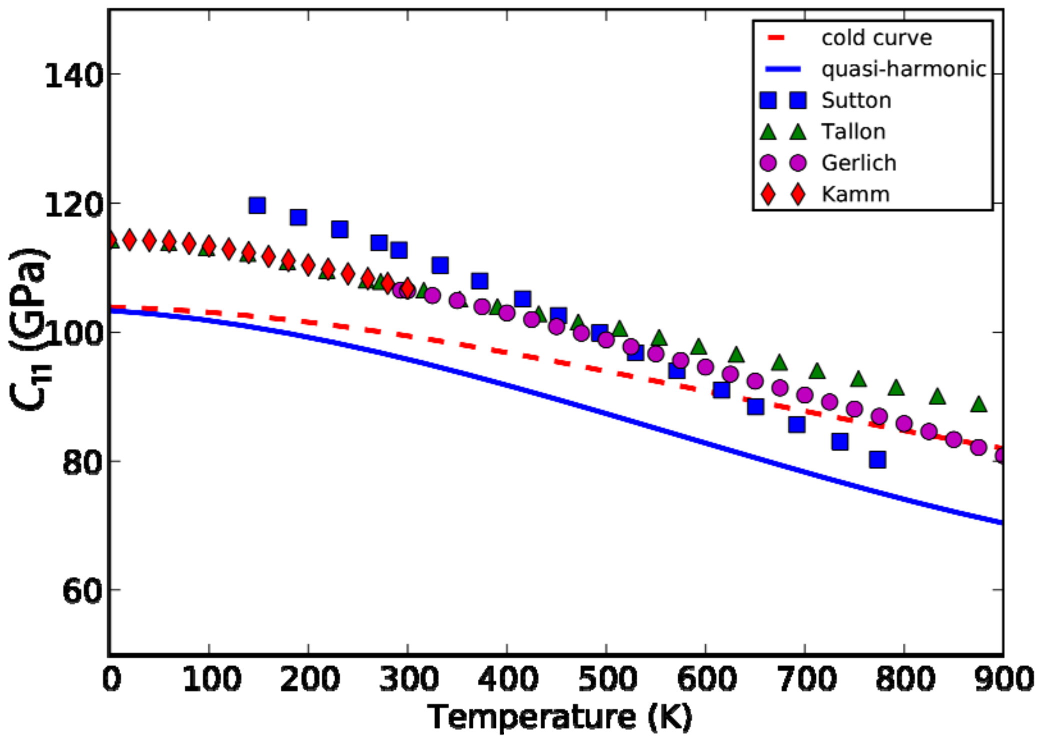

FIG. 2. (color online) Experimental[2-5] and DFT calculated C_{11} adiabatic elastic constant. For the curve labeled as ‘cold curve’ (solid, blue line), the elastic constants where calculated from the strain-energy relations at 0 K at different volumes. Ab initio-calculated volume expansion was then used to convert volume to temperature dependence. The curve labeled as quasi-harmonic was obtained from strain-free energy relations.

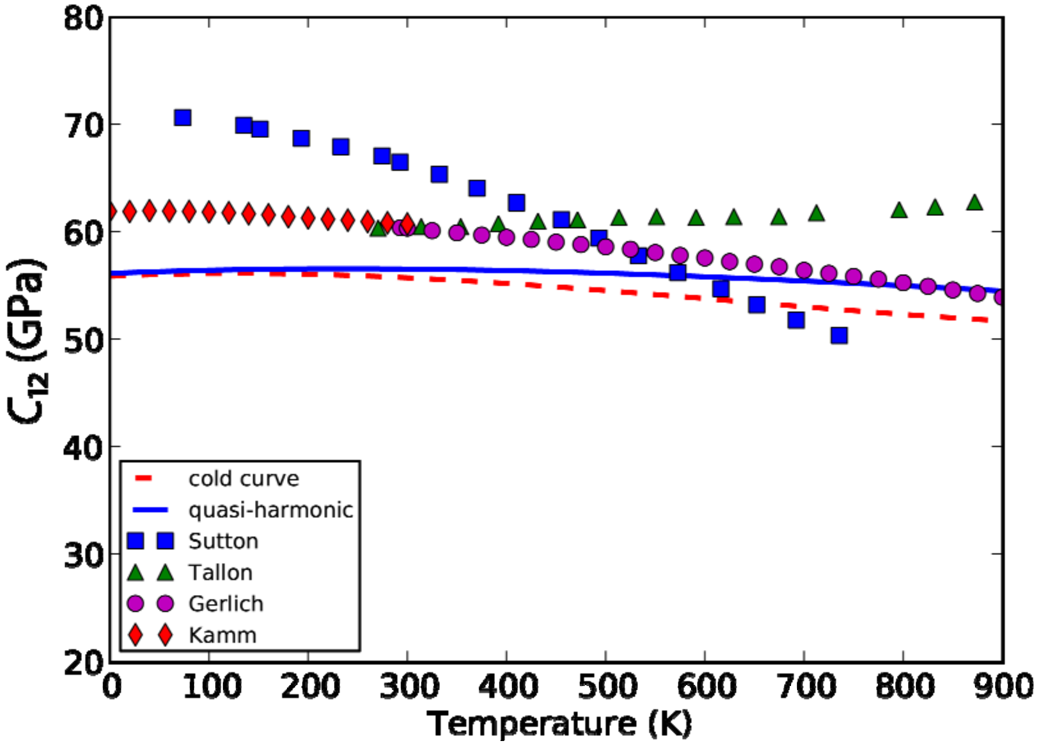

FIG. 3. (color online) Experimental[2-5] and DFT calculated C_{12} adiabatic elastic constant. For the curve labeled as 'cold curve' (solid, blue line), the elastic constants where calculated from the strain-energy relations at 0K at different volumes. Ab initio-calculated volume expansion was then used to convert volume to temperature dependence. The curve labeled as quasi-harmonic was obtained from strain-free energy relations.

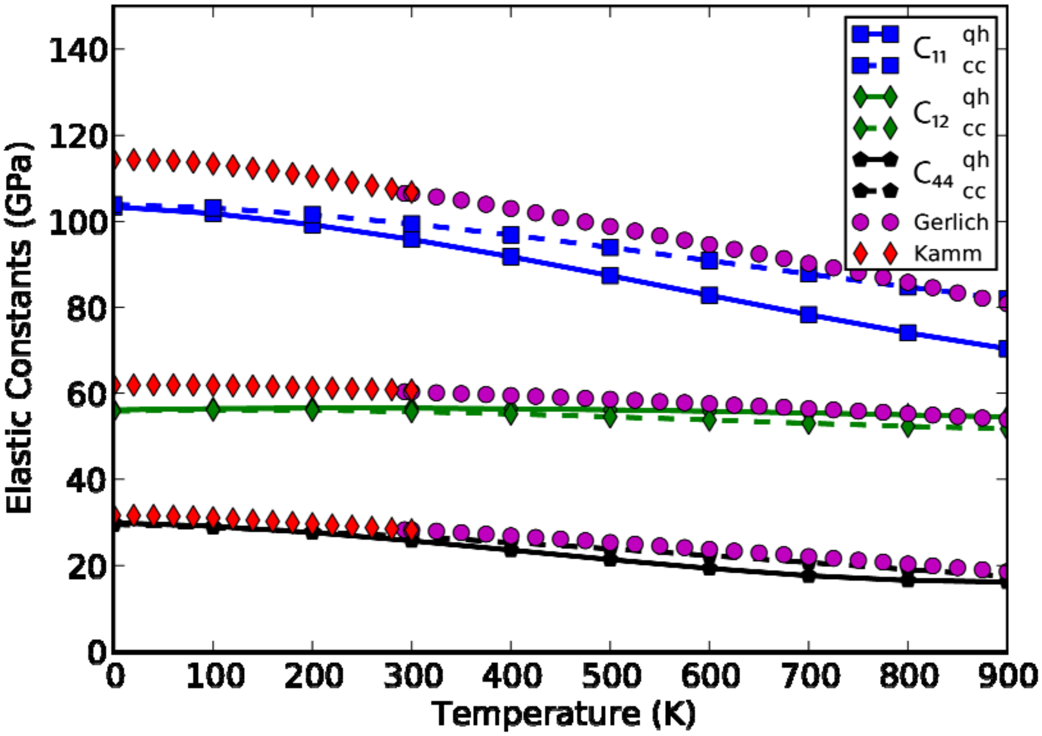

FIG. 4. (color online) DFT calculated and experimental[2, 3] adiabatic elastic constants of fcc Al. For the curves labeled as 'cold curve' (solid, blue line), the elastic constants where calculated from the strain-energy relations at 0 K at different volumes. Ab initio-calculated volume expansion was then used to convert volume to temperature dependence. The curves labeled as quasi-harmonic was obtained from strain-free energy relations.

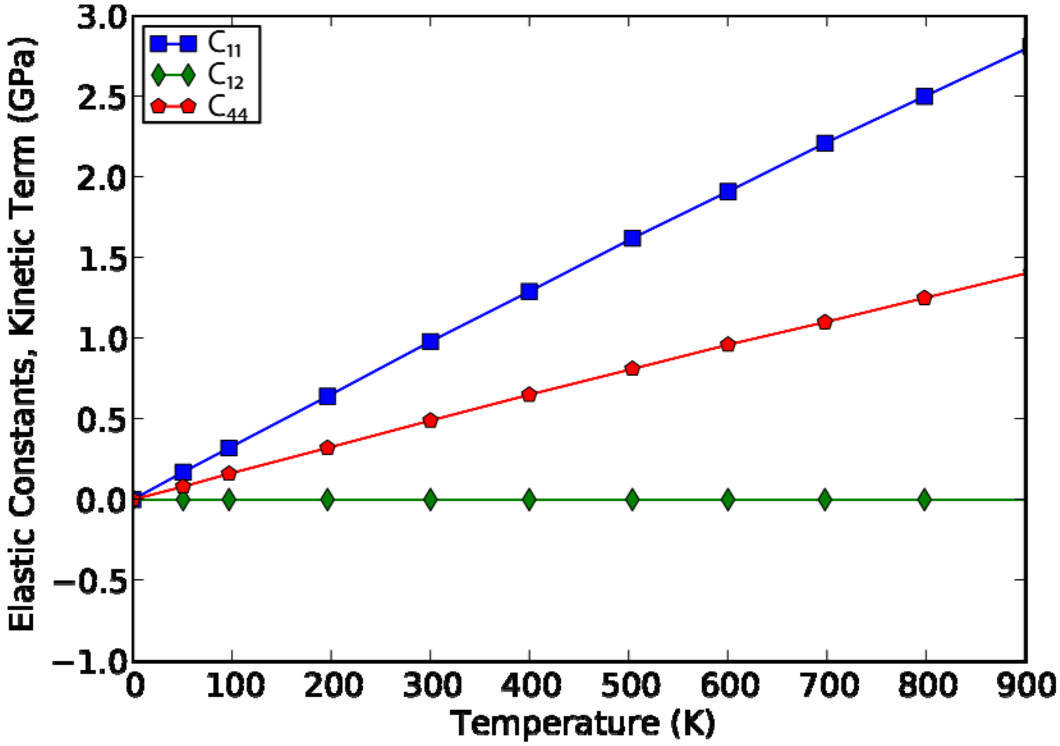

FIG. 5. (color online) Kinetic energy contributions to C_{11}, C_{12}, C_{44} as a function of temperature in MD calculations.

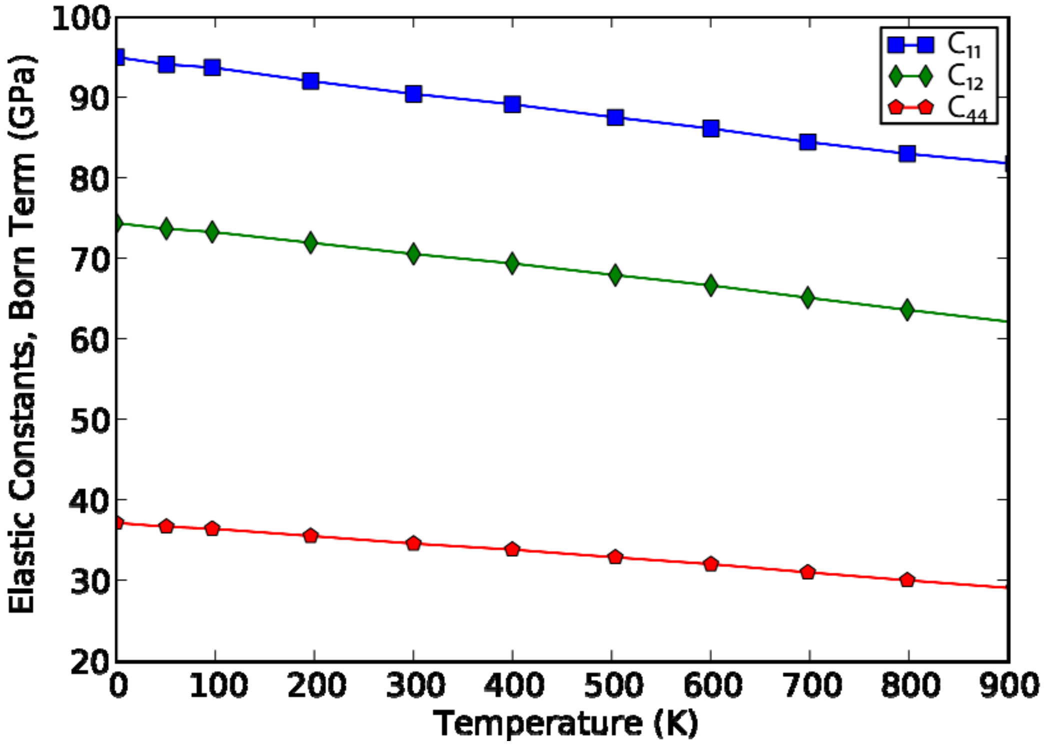

FIG. 6. (color online) Born term contributions to C_{11}, C_{12}, C_{44} as a function of temperature in MD calculations.

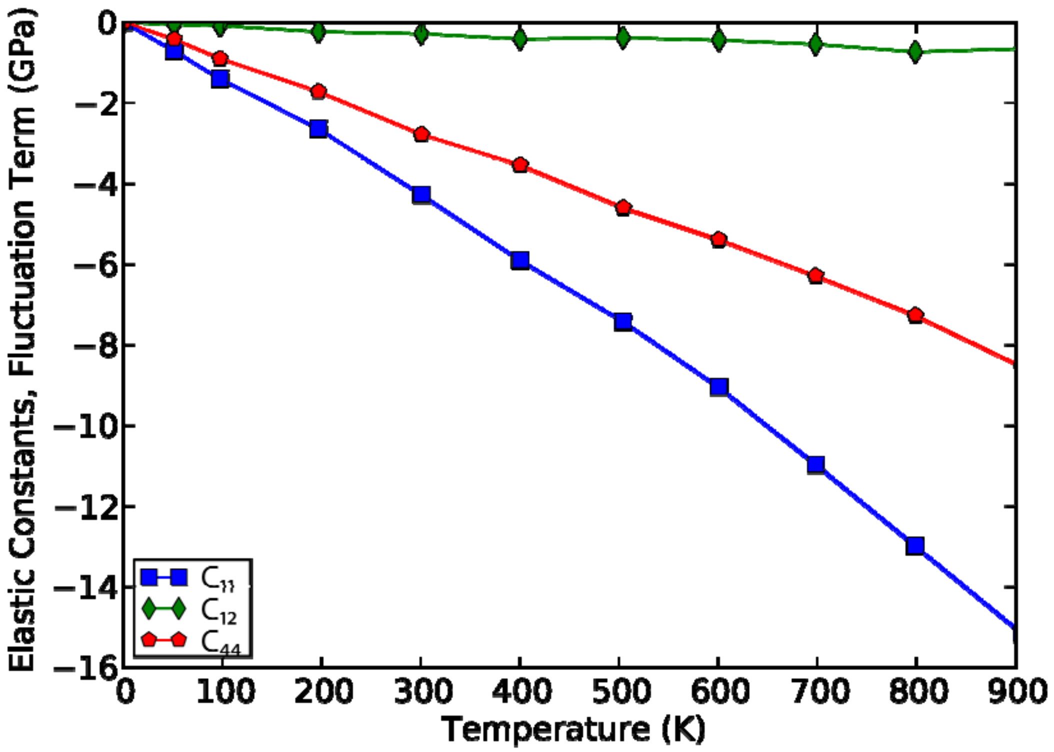

FIG. 7. (color online) Fluctuation term contributions to C_{11}, C_{12}, C_{44} as a function of temperature in MD calculations.

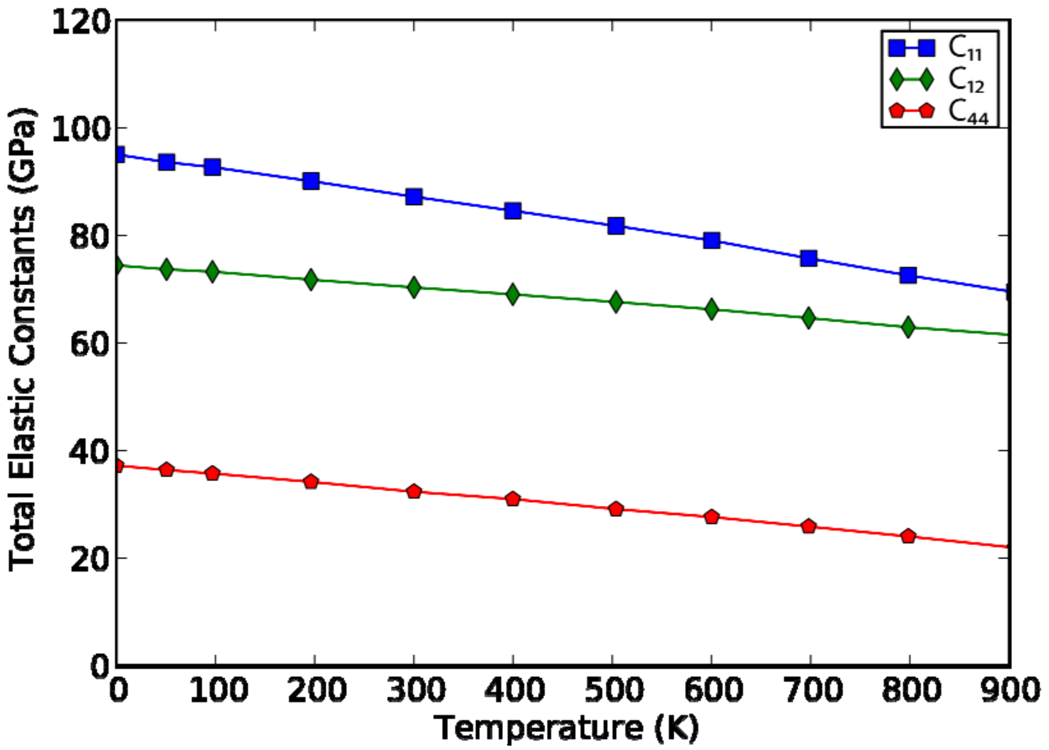

FIG. 8. (color online) MD calculations on C_{11}, C_{12}, C_{44} at elevated temperatures.

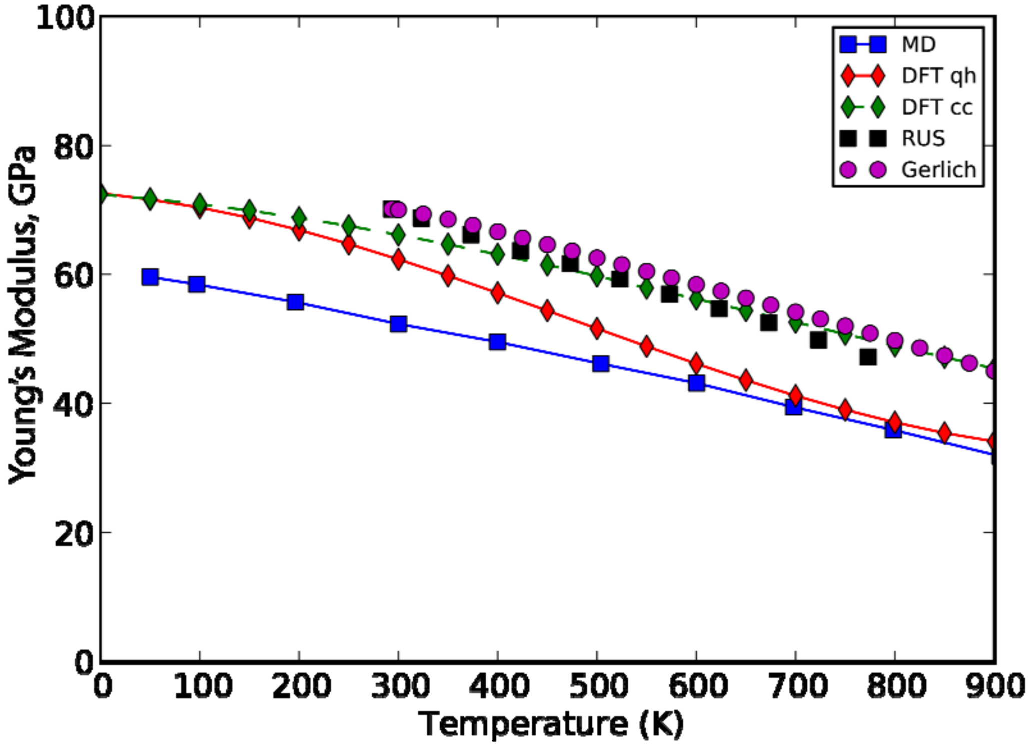
Young's Modulus, GPa
100
80
60
40
20
0
Temperature (K)
0
100
200
300
400
500
600
700
800
900
MD
DFT qh
DFT cc
RUS
Gerlich

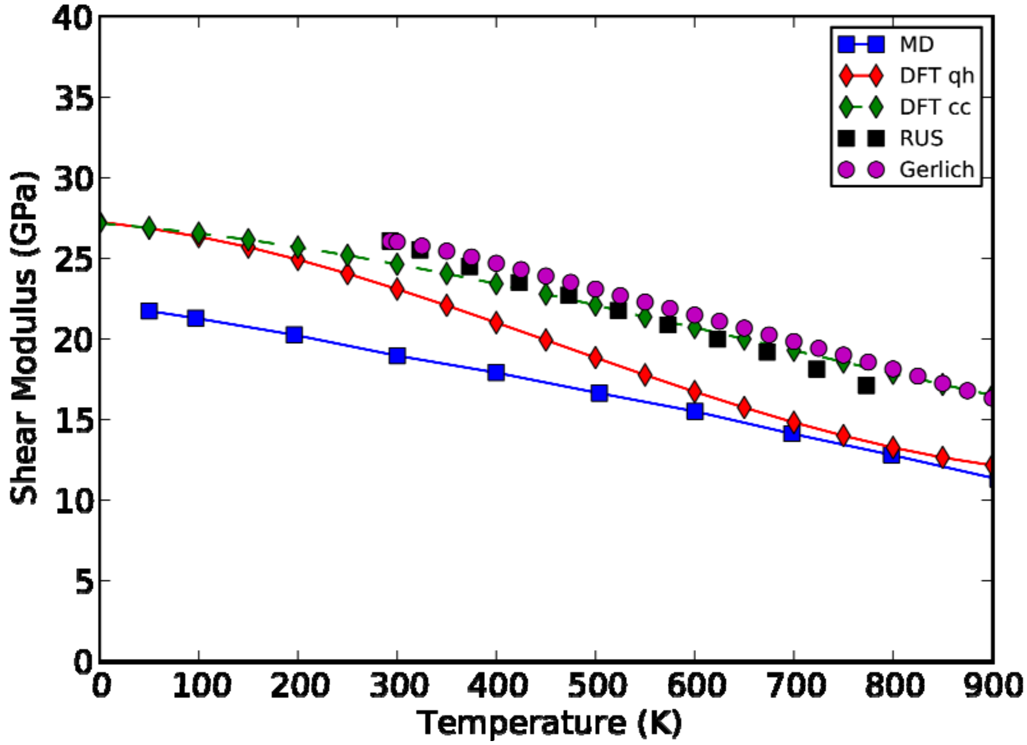
Shear Modulus (GPa)
40
35
30
25
20
15
10
5
0
Temperature (K)
0
100
200
300
400
500
600
700
800
900
MD
DFT qh
DFT cc
RUS
Gerlich

FIG. 9. (color online) Polycrystalline Young's (a) and shear modulus (b). The averaged elastic constants from experimental results by Gerlich[2] as well as those measured in this work through RUS are compared to DFT and classical MD calculations.

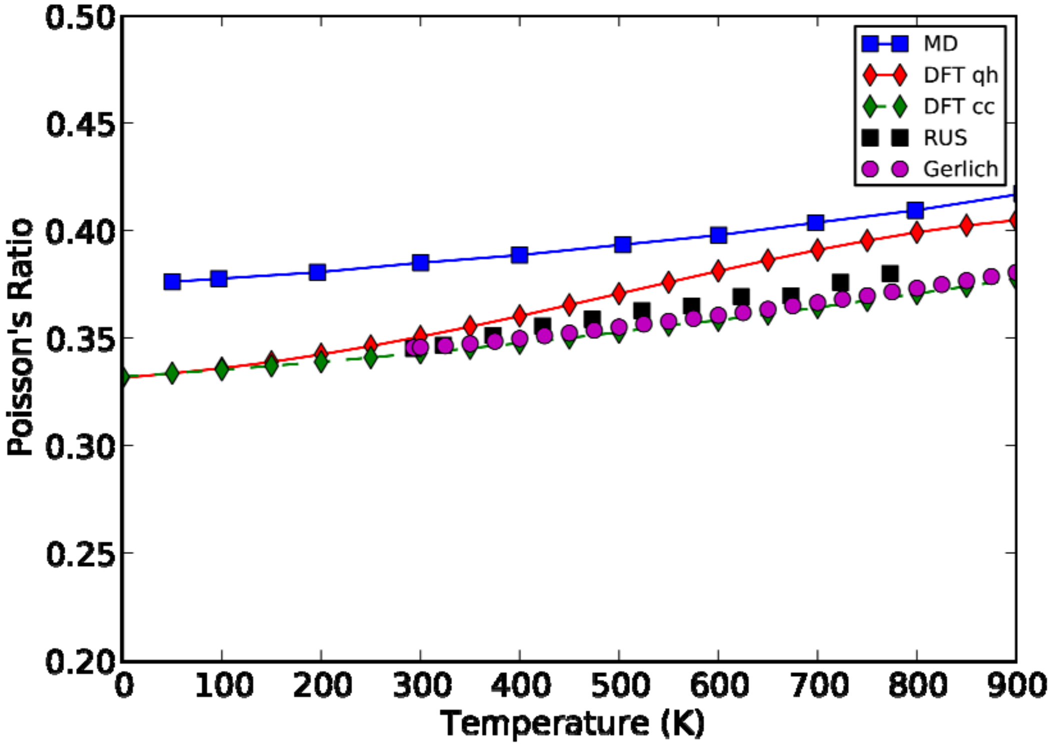

FIG. 10. (color online) Polycrystalline Poisson's ratio. The averaged elastic constants from experimental results by Gerlich[2] as well as those measured in this work through RUS are compared to DFT and classical MD calculations.